Received: 26 March 2025 | Revised: 19 June 2025 | Accepted: 18 July 2025

DOI: 10.1002/aic.70016

RESEARCH ARTICLE

Process Systems Engineering

AIChE JOURNAL

Minimum reflux calculation for multicomponent distillation in multi-feed, multi-product columns: Algorithms and examples

Zheyu Jiang [1,2] | Mohit Tawarmalani [3] | Rakesh Agrawal [1]

[1]Davidson School of Chemical Engineering, Purdue University, West Lafayette, Indiana, USA

[2]School of Chemical Engineering, Oklahoma State University, Stillwater, Oklahoma, USA

[3]Mitch Daniels School of Business, Purdue University, West Lafayette, Indiana, USA

Correspondence

Zheyu Jiang, School of Chemical Engineering, Oklahoma State University, Stillwater, Oklahoma, USA.
Email: zjiang@okstate.edu

Mohit Tawarmalani, Mitch Daniels School of Business, Purdue University, West Lafayette, IN 47907, USA.
Email: mtawarma@purdue.edu

Rakesh Agrawal, Davidson School of Chemical Engineering, Purdue University, West Lafayette, IN 47907, USA.
Email: agrawalr@purdue.edu

Abstract

In this work, we present the first algorithm for identifying the minimum reboiler vapor duty requirement for a general multi-feed, multi-product (MFMP) distillation column separating ideal multicomponent mixtures. This algorithm incorporates our recently developed shortcut model for MFMP columns. We demonstrate the accuracy and efficiency of this algorithm through case studies. The results obtained from these case studies provide valuable insights into the optimal design of MFMP columns. Many of these insights go against the existing design guidelines and heuristics. For example, placing a colder saturated feed stream above a hotter saturated feed stream sometimes leads to a higher energy requirement. Furthermore, decomposing a general MFMP column into individual simple columns may lead to incorrect estimation of the minimum reflux ratio for the MFMP column. Thus, the algorithm presented here offers a fast, accurate, and automated approach to synthesize new, energy-efficient, and cost-effective MFMP columns.

KEYWORDS

minimum reflux ratio, multi-feed and multi-product distillation column, Multicomponent distillation, optimization, Underwood method

1 | INTRODUCTION

Distillation is a ubiquitous separation technology in the chemical process industries, consuming almost 50% of the energy used by the chemical industries and about 40% by the refining process.[1,2] Assuming that 50% of the CO_2 equivalent release from process heating in chemical manufacturing and 40% in petroleum refining are attributable to distillation, distillation alone would be responsible for 95 million tons of CO_2 release in the U.S. each year.[3] Thus, a reduction in distillation energy consumption also leads to reduced carbon footprint.[4]

While binary mixtures can generally be separated using one distillation column, multicomponent mixtures, which are more commonly encountered in industrial separations, require a sequence of columns called a distillation configuration to achieve the desired separation. As the number of components in the feed increases, the total number of possible distillation configurations increases combinatorially.[5] Among these distillation configurations, many contain one or more distillation columns with multiple feed streams and/or one or more side-draw product streams. These configurations with multi-feed, multi-product (MFMP) columns (see Figure 1 for an example) are well-known to be more energy-efficient than the "sharp-split configurations" which do not include any MFMP columns.[6,7]

MFMP columns can also be derived from conventional one-feed, two-product columns in binary and multicomponent distillation by applying various process intensification techniques,[8–10] including heat pumps,[11,12] double and multi-effect,[13] intermediate reboilers and condensers,[14] prefractionator arrangement,[15] feed preconditioning,[16]

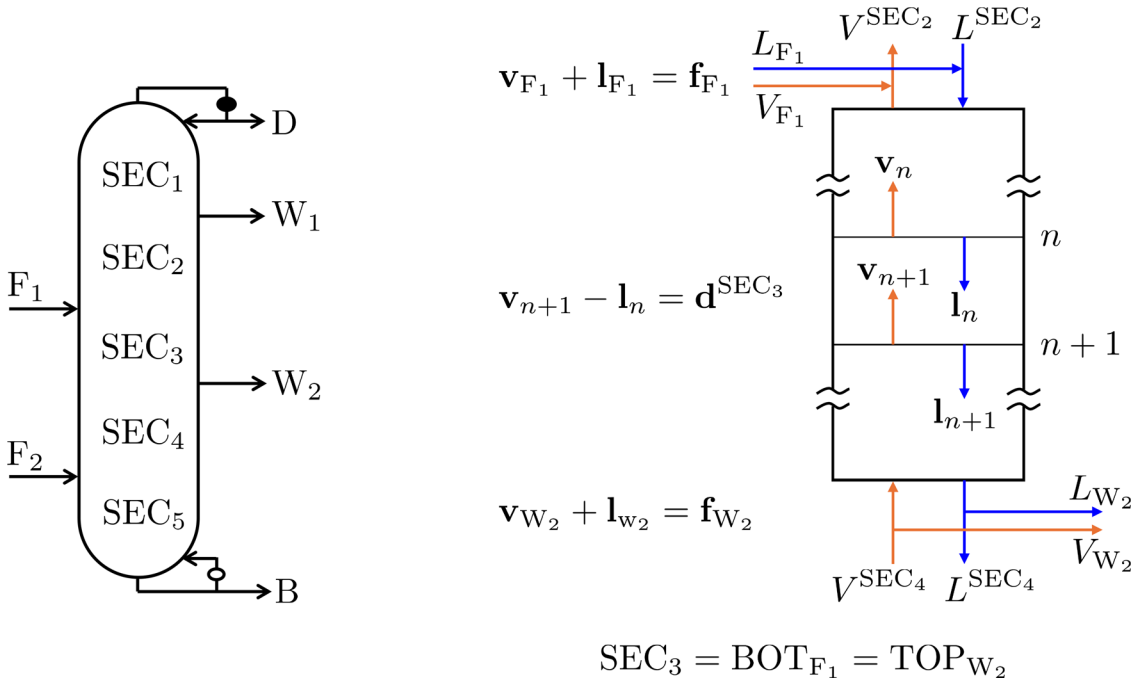

FIGURE 1 An example MFMP column with three feed streams and two sidedraw product streams and a detailed illustration of liquid and vapor flows within SEC_3, in which the variables in bold are component flow vectors (e.g., $\mathbf{d}^{sec_3} = (d_1^{sec_3}, ..., d_c^{sec_3})$ for a c-component system). The column section is numbered from top (1) to bottom ($N_{SEC} = 5$). The definitions of variables and parameters used here and for the rest of this paper are summarized in Online Appendices A and B. We follow the convention that $\mathbf{v}_{F_j}$, $\mathbf{l}_{F_j}$, and $\mathbf{f}_{F_j} \geq \mathbf{0}$, whereas $\mathbf{v}_{W_j}$, $\mathbf{l}_{W_j}$, and $\mathbf{f}_{W_j} \leq \mathbf{0}$.

heat and mass integration,[17] and so on. Compared to the original conventional columns, these new MFMP columns not only require significantly less energy from the perspective of the first law of thermodynamics, but have much higher thermodynamic efficiency from the second-law perspective,[18] making them more attractive than alternative technologies for a variety of industrial separations.[10,19] Thus, MFMP columns are becoming increasingly important in the context of industrial decarbonization and a net-zero economy, as they can provide substantial energy-saving benefits.

The minimum reflux ratio of a distillation column closely relates to its energy consumption, capital cost, and operational limit[20,21] and is a key parameter in distillation design and operation. Naively determining a column's minimum reflux ratio by performing exhaustive sensitivity analysis using process simulators is a tedious task that often faces convergence issues. Instead, a fast and accurate algorithmic approach to calculate the actual minimum reflux condition of a general MFMP column opens up an opportunity to design new, energy-efficient, and cost-effective multicomponent distillation systems. Ideally, such a method should also have a simple mathematical formulation that can be easily incorporated in a (global) optimization framework for fast and accurate identification of attractive configurations from an enormous configuration search space.

Over the past decades, a number of algorithmic methods have been proposed to determine the minimum reflux ratio of a general MFMP column accurately and efficiently. A comprehensive review of these methods can be found in the first article of this series.[22] However, these methods either rely on several simplifying assumptions—some of which are too restrictive and often incorrect—or require rigorous tray-by-tray calculations, which are computationally prohibitive to be practical for evaluating a large number of configurations. To fill this gap, in our previous work,[22] we developed the first shortcut mathematical model to analytically determine the minimum reflux ratio of any general MFMP column entirely assuming ideal vapor-liquid equilibrium (VLE), constant relative volatility (CRV), and constant molar overflow (CMO). Our shortcut model is fully generalized as it works for any MFMP column with no particular requirement on feed and/or sidedraw arrangement or product composition specification. Also, the proposed shortcut model does not involve any tray-by-tray calculations. Moreover, the physical and mathematical properties associated with the shortcut model are explored, from which we successfully derive the mathematical conditions for any general MFMP column operated at minimum reflux. In addition, relaxations of the ideal VLE, CRV, and CMO assumptions have been investigated recently without changing the general mathematical structure of the governing equation,[23–26] hence extending the flexibility and applicability of our shortcut model to real multicomponent systems even further while preserving the mathematical properties and minimum reflux conditions of our shortcut model. Specifically, Mathew et al.[23] recently relaxed the CMO assumption in the shortcut model to constant heat flow (CHT) to account for different latent heats in multicomponent systems. This extension allows us to identify energy-efficient multicomponent distillation configurations based on heat

duty rather than surrogate vapor flow. Mathew et al.[24,25] and Tumbalam Gooty et al.[26] relaxed the original definitions of CRV and ideal VLE assumptions by considering it as a surrogate model for the true VLE behavior of real zeotropic mixtures, rather than an assumption just for ideal mixtures. This means that, for most ideal and nonlinear zeotropic mixtures containing c components, the vapor composition of any component $i \in \mathcal{C} = \{1,...,c\}$ across its entire composition range follows the relation:

$$y_i = \frac{\alpha_i x_i}{\sum_{j=1}^{c} \alpha_j x_j}, \tag{1}$$

where x_i is the liquid composition in equilibrium with y_i and $\{\alpha_j\}_j$ is a set of constant relative volatility values that are obtained by nonlinear least-square regression using experimental VLE data. On a side note, we remark that our shortcut model can even be extended for homogeneous azeotropic systems. For example, Jiang[27] followed a similar derivation procedure as Jiang et al.[22] and successfully extended the shortcut model to homogeneous azeotropic mixtures and derived the minimum reflux condition for simple columns. More recently, Taifan and Maravelias[28] derived essentially the same shortcut model for homogeneous azeotropic distillation in parallel and introduced an optimization framework to synthesize attractive azeotropic distillation configurations.

Here, we introduce an algorithmic method that incorporates the shortcut model developed earlier to efficiently and accurately determine the minimum reboiler vapor duty requirement for a general MFMP column separating a multicomponent mixture. This algorithm can be used by itself to find the minimum reflux condition for a standalone MFMP column, or can be embedded into a global optimization framework[7,18,29,30] to simultaneously optimize an entire configuration consisting of one or more MFMP columns. Later, we present three case studies providing comparisons with rigorous Aspen Plus simulations to illustrate the accuracy and usefulness of our algorithm. Also, we show that results from these case studies could challenge some of the widely used design heuristics and rules of thumb that researchers and practitioners have been using. Thus, our shortcut method and the minimum reflux calculation algorithm presented here provide new perspectives on how to accurately model, design, and operate MFMP columns.

2 | A BRIEF SUMMARY OF SHORTCUT MODEL FOR MFMP COLUMNS

Before we introduce the minimum reflux calculation algorithm for MFMP columns, we first review the shortcut model we developed earlier[22] and some of its key consequences. This includes the mathematical conditions that dictate whether the target separation task can be achieved (with a finite or infinite number of stages) in the MFMP column. Our previous work[22] provides detailed derivations and explanations of these results. We consider a column section, which is separated by either a feed or a product stream, as the smallest module of an MFMP column. The idea is that, by constructing a shortcut model of a column section and exploring its mathematical and physical properties, we can derive a set of algebraic constraints that must be satisfied for each and every pair of adjacent column sections to maintain connectivity of the (liquid) composition profile between any adjacent sections, hencing enforcing the feasibility of separation of the entire MFMP column. In particular, when the target separation can only be achieved by requiring an infinite number of stages (i.e., some column sections have to be pinched), then the corresponding reflux ratio is the minimum reflux ratio of the MFMP column with respect to the target separation goal.

Consider an MFMP column with N_{SEC} number of column sections separated by N_F number of feed and N_W number of sidedraw streams (note that $N_{SEC} = N_F + N_W + 1$). Following the nomenclature used in our previous work[22] and herein summarized in Online Appendices A and B, for a c-component system, let $\alpha_c > \alpha_{c-1} > \cdots > \alpha_1 = 1$ be the relative volatilities with respect to the least volatile component (Component 1) obtained by fitting the VLE using least-square regression to closely capture the true VLE behavior. Given the feed and product flow rate and composition specifications, we can determine the net material upward flow for component i in column section k, namely $d_i^{SEC_k}$ (see Figure 1). Then, for a specific section vapor flow V^{SEC_k}, we can solve the following equation[22] to obtain a total of c roots, $\{\gamma_i^{SEC_k}\}_{i \in \mathcal{C}}$:

$$\sum_{i=1}^{c} \frac{\alpha_i d_i^{SEC_k}}{\alpha_i - \gamma^{SEC_k}} = V^{SEC_k}. \tag{2}$$

Suppose $d_c,...,d_l > 0$, $d_{l-1},...,d_{h+1} = 0$, and $d_h,...,d_1 < 0$ for some $1 \le h < l \le c$ in a column section. In other words, more volatile components $c,...,l$ have net material upward flows, intermediately volatile components $l-1,...,h+1$ have net zero material flows, and less volatile components $h,...,1$ have net material downward flows. It can be verified that all c roots lie in the following intervals:

$$\begin{aligned} \gamma_i^{SEC_k} &\in (\alpha_i, \alpha_{i+1}) && \text{for } i \in \{1,...,h\} \\ \gamma_i^{SEC_k} &= \alpha_i && \text{for } i \in \{h+1,...,l-1\} \\ \gamma_i^{SEC_k} &\in (\alpha_{i-1}, \alpha_i) && \text{for } i \in \{l,...,c\}. \end{aligned} \tag{3}$$

As for the edge cases, when $l = h+1$, meaning that there are no intermediate components with net zero material flows, there are two roots in the interval $(\alpha_h, \alpha_l) = (\alpha_h, \alpha_{h+1})$ and exactly one root in each of the remaining $c-1$ relative volatility intervals (see Figure 2). It turns out that the pinch root $\gamma_p^{SEC_k}$ (the subscript p stands for "pinch" and its value corresponds to the pinch index), which determines the actual pinch zone composition in SEC_k, actually lies in (α_h, α_l). That is, the pinch root lies in a relative volatility interval where the sign change in d_i occurs.[22]

For the second edge case, when $h = 0$, meaning that all components have non-negative net material upward flow in SEC_k, we have $\gamma_i^{SEC_k} = \alpha_i$ for $i \in \{1,...,l-1\}$ and $\gamma_i^{SEC_k} \in (\alpha_{i-1}, \alpha_i)$ for $i \in \{l,...,c\}$. In this case, the pinch root $\gamma_p^{SEC_k} = \gamma_l^{SEC_k} \in (\alpha_{l-1}, \alpha_l)$. Additionally, if $l = 1$,

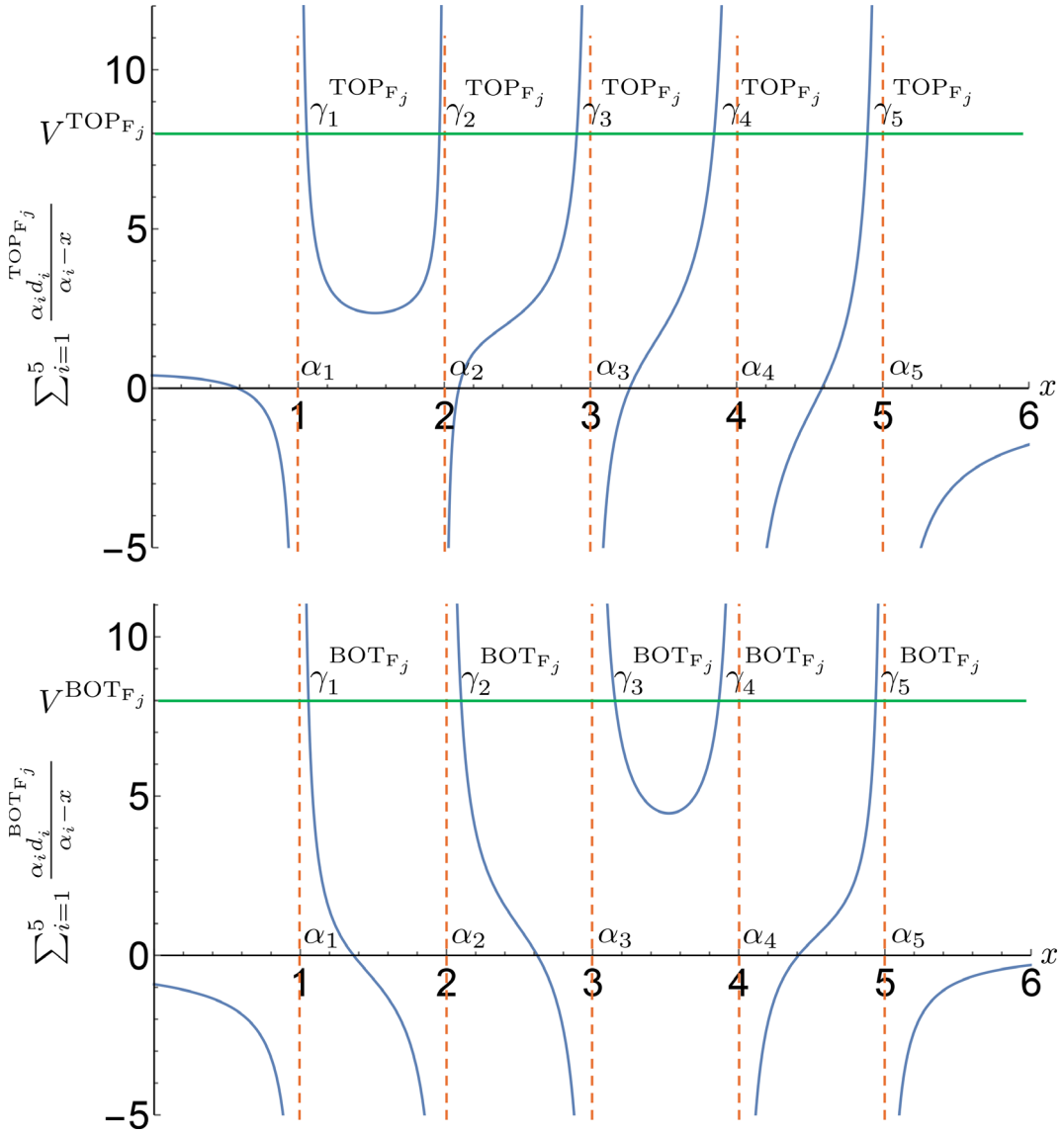

FIGURE 2 Roots of Equation (2) for a five-component illustrative example where $(d_1,d_2,d_3,d_4,d_5)=(-0.4,0.1,0.2,0.3,0.2)$ for section $\mathrm{TOP}_{\mathrm{F}j}$, $(d_1,d_2,d_3,d_4,d_5)=(-0.4,0.1,0.2,0.3,0.2)$ for feed $\mathrm{TOP}_{\mathrm{F}j}$, and $(d_1,d_2,d_3,d_4,d_5)=(-0.5,-0.4,-0.3,0.2,0.1)$ for section $\mathrm{BOT}_{\mathrm{F}j}$. The relative volatilities are $(\alpha_1,\alpha_2,\alpha_3,\alpha_4,\alpha_5)=(1,2,3,4,5)$. The section vapor flow V is set to be 8, and F_j is a saturated liquid. In this case, the pinch roots $\gamma_p^{\mathrm{TOP}_{\mathrm{F}j}}\in(\alpha_1,\alpha_2)$ and $\gamma_p^{\mathrm{BOT}_{\mathrm{F}j}}\in(\alpha_3,\alpha_4)$.

meaning that all components have net material upward flow in the column section, we have $\gamma_i^{\mathrm{SEC}_k}\in(\alpha_{i-1},\alpha_i)$ for $i\in\mathcal{C}$, where α_0 is defined as 0. And the pinch root $\gamma_p^{\mathrm{SEC}_k}=\gamma_1^{\mathrm{SEC}_k}\in(\alpha_0,\alpha_1)$.

Lastly, when $l=c+1$, meaning that all components have non-positive net material upward flow in SEC_k, we have $\gamma_i^{\mathrm{SEC}_k}\in(\alpha_i,\alpha_{i+1})$ for $i\in\{1,\ldots,h\}$ and $\gamma_i^{\mathrm{SEC}_k}=\alpha_i$ for $i\in\{h+1,\ldots,c\}$. In this case, the pinch root $\gamma_p^{\mathrm{SEC}_k}=\gamma_h^{\mathrm{SEC}_k}\in(\alpha_h,\alpha_{h+1})$. Additionally, if $h=c$, meaning that all components have net material downward flow in the column section, we have $\gamma_i^{\mathrm{SEC}_k}\in(\alpha_i,\alpha_{i+1})$ for $i\in\mathcal{C}$. Here, we denote $\alpha_{c+1}=\alpha_c+\delta$, where δ is set to be a sufficient large number. And the pinch root $\gamma_p^{\mathrm{SEC}_k}=\gamma_c^{\mathrm{SEC}_k}\in(\alpha_c,\alpha_{c+1})$.

Now that we have reviewed the key results of our shortcut model, in the next section, we will derive the algorithmic formulation to determine the minimum reflux ratio or minimum reboiler vapor duty for a general MFMP column.

3 | MINIMUM REFLUX CONDITION FORMULATION FOR MFMP COLUMNS

Recall that for c-component system, the domain of $\gamma_i^{\mathrm{SEC}_k}$ roots to Equation (2) can be split into $c+1$ distinct intervals: $(0,\alpha_1)$, (α_1,α_2), ..., (α_{c-1},α_c), and $(\alpha_c,\alpha_c+\delta)$, where δ is a sufficiently large positive number. The pinch root $\gamma_p^{\mathrm{SEC}_k}$ for SEC_k must lie in one of these $c+1$ intervals. Thus, we may define a set of binary variables $\{\mu_i^{\mathrm{SEC}_k}\in\{0,1\}\}_{i=1}^{c+1}$, where $\mu_i^{\mathrm{SEC}_k}=1$ when the pinch root $\gamma_p^{\mathrm{SEC}_k}\in(\alpha_{i-1},\alpha_i)$, and is 0

otherwise. Here, we denote $\alpha_0 = 0$. This way, the pinch root must satisfy the following constraints:

$$\begin{aligned} &\sum_{i=1}^{c+1} \alpha_{i-1}\mu_i^{\mathrm{SEC}_k} \le \gamma_p^{\mathrm{SEC}_k} \le \sum_{i=1}^{c+1} \alpha_i \mu_i^{\mathrm{SEC}_k} \\ &\sum_{i=1}^{c+1} \mu_i^{\mathrm{SEC}_k} = 1 \end{aligned} \quad \forall k = 1,\ldots,N_{\mathrm{SEC}}. \tag{4}$$

When two adjacent column sections are separated by a feed stream F_j ($j = 1,\ldots,N_{\mathrm{F}}$), we denote the section above F_j as $\mathrm{TOP}_{\mathrm{F}j}$ and the one below as $\mathrm{BOT}_{\mathrm{F}j}$ (see Figure 1). Since $d_i^{\mathrm{TOP}_{\mathrm{F}j}} - d_i^{\mathrm{BOT}_{\mathrm{F}j}} = f_{i,\mathrm{F}_j} \ge 0$, we have $d_i^{\mathrm{TOP}_{\mathrm{F}j}} \ge d_i^{\mathrm{BOT}_{\mathrm{F}j}}$ for $i \in \mathcal{C}$, indicating that the pinch index for $\mathrm{TOP}_{\mathrm{F}j}$ would be at most the same as the pinch index for $\mathrm{BOT}_{\mathrm{F}j}$, hence satisfying $p^{\mathrm{TOP}_{\mathrm{F}j}} \le p^{\mathrm{BOT}_{\mathrm{F}j}}$, or:

$$\sum_{i=1}^{c+1} i\mu_{i,\mathrm{BOT}_{\mathrm{F}j}} \ge \sum_{i=1}^{c+1} i\mu_{i,\mathrm{TOP}_{\mathrm{F}j}} \quad \forall j = 1,\ldots,N_{\mathrm{F}}. \tag{5}$$

We define an index set $\mathcal{I}_{\mathrm{F}_j}$ storing all indices of intervals ranging from $\max\{2, \sum_{i=1}^{c+1} i\mu_{i,\mathrm{TOP}_{\mathrm{F}j}}\}$ to $\min\{c, \sum_{i=1}^{c+1} i\mu_{i,\mathrm{BOT}_{\mathrm{F}j}}\}$ (i.e., considering intervals within α_1 and α_c and excluding the two intervals (α_0,α_1) and (α_c,α_{c+1})). To better characterize $\mathcal{I}_{\mathrm{F}_j}$, we define a new set of binary variables $\{K_i^{\mathrm{SEC}_k} \in \{0,1\}\}_{i=1}^{c+1}$ for column section k where:

$$K_i^{\mathrm{SEC}_k} = \sum_{m=1}^{i} \mu_m^{\mathrm{SEC}_k} \quad \forall i = 1,\ldots,c+1;\ k = 1,\ldots,N_{\mathrm{SEC}}. \tag{6}$$

Clearly, $K_i^{\mathrm{SEC}_k} = 0$ if and only if $\mu_1^{\mathrm{SEC}_k},\ldots,\mu_i^{\mathrm{SEC}_k}$ are all equal to 0. And $K_i^{\mathrm{SEC}_k}$ changes from 0 to 1 at index i where $\mu_i^{\mathrm{SEC}_k} = 1$ (i.e., $\gamma_p^{\mathrm{SEC}_k} \in (\alpha_{i-1},\alpha_i)$) and then stays at 1 for indices greater than i. Knowing this, it can be verified that $\mathcal{I}_{\mathrm{F}_j}$ can be equivalently expressed as:

$$\mathcal{I}_{\mathrm{F}_j} = \{i \in \mathcal{C} | K_i^{\mathrm{TOP}_{\mathrm{F}j}} - K_{i-1}^{\mathrm{BOT}_{\mathrm{F}j}} = 1\} \quad \forall j = 1,\ldots,N_{\mathrm{F}}. \tag{7}$$

For example, consider the same five-component system whose root profiles for $\mathrm{TOP}_{\mathrm{F}j}$ and $\mathrm{BOT}_{\mathrm{F}j}$ are shown in Figure 2. Correspondingly, the relationship between mu_i and K_i variables for this illustrative example is shown in Figure 3. Following Equation (7), we have $\mathcal{I}_{\mathrm{F}_j} = \{2,3,4\}$.

With this, one of the key results obtained in our previous work[22] is that, the feasibility of the target separation requires the following constraint to the satisfies in sections $\mathrm{TOP}_{\mathrm{F}j}$ and $\mathrm{BOT}_{\mathrm{F}j}$ for every $i \in \mathcal{I}_{\mathrm{F}_j}$:

$$\gamma_i^{\mathrm{TOP}_{\mathrm{F}j}} \ge \rho_{i-1,\mathrm{F}_j} \ge \gamma_{i-1}^{\mathrm{BOT}_{\mathrm{F}j}} \quad \forall i \in \mathcal{I}_{\mathrm{F}_j};\ j = 1,\ldots,N_{\mathrm{F}} \tag{8}$$

where $\{\rho_{i-1,\mathrm{F}_j}\}_{i \in \mathcal{I}_{\mathrm{F}_j}}$ satisfy:

$$\sum_{m=1}^{c} \frac{\alpha_m l_{m,\mathrm{F}_j}}{\alpha_m - \rho_{i-1,\mathrm{F}_j}} = 0 \quad \text{or} \quad \sum_{m=1}^{c} \frac{\alpha_m f_{m,\mathrm{F}_j}}{\alpha_m - \rho_{i-1,\mathrm{F}_j}} = V_{\mathrm{F}_j} \quad j = 1,\ldots,N_{\mathrm{F}}. \tag{9}$$

Here, $\rho_{i-1,\mathrm{F}_j} \in (\alpha_{i-1},\alpha_i)$. Here, $l_{m,\mathrm{F}_j} \ge 0$, $f_{m,\mathrm{F}_j} \ge 0$, and $V_{\mathrm{F}_j} \ge 0$ correspond to the flow rate of component m in the liquid portion of F_j, the feed flow rate of component m, and the total vapor flow rate of the feed, respectively. When F_j is in saturated vapor state, then l_{m,F_j} represents the hypothetical liquid feed flow that is in thermodynamic equilibrium with the vapor feed[22] based on Equation (1):

$$l_{m,\mathrm{F}_j} = \frac{\frac{v_{m,\mathrm{F}_j}}{\alpha_m}}{\sum_{k=1}^{c} \frac{v_{k,\mathrm{F}_j}}{\alpha_k}} \quad \forall m \in \mathcal{C}.$$

To implement Equation (8) algorithmically, we leverage the fact that $K_i^{\mathrm{TOP}_{\mathrm{F}j}} - K_{i-1}^{\mathrm{BOT}_{\mathrm{F}j}}$ is itself a binary variable indicating whether index $i \in \mathcal{I}_{\mathrm{F}_j}$ or not. Thus, Equation (8) can be rewritten as:

$$\begin{aligned} &(K_i^{\mathrm{TOP}_{\mathrm{F}j}} - K_{i-1}^{\mathrm{BOT}_{\mathrm{F}j}})(\gamma_i^{\mathrm{TOP}_{\mathrm{F}j}} - \rho_{i-1,\mathrm{F}_j}) \ge 0 \\ &(K_i^{\mathrm{TOP}_{\mathrm{F}j}} - K_{i-1}^{\mathrm{BOT}_{\mathrm{F}j}})(\rho_{i-1,\mathrm{F}_j} - \gamma_{i-1}^{\mathrm{BOT}_{\mathrm{F}j}}) \ge 0 \end{aligned} \quad \forall i \in \mathcal{C} \setminus \{1\};\ j = 1,\ldots,N_{\mathrm{F}}. \tag{10}$$

When two adjacent column sections are connected by a sidedraw stream W_j ($j = 1,\ldots,N_{\mathrm{W}}$), we denote the section above W_j as $\mathrm{TOP}_{\mathrm{W}j}$ and the one below as $\mathrm{BOT}_{\mathrm{W}j}$. Since $d_i^{\mathrm{TOP}_{\mathrm{W}j}} - d_i^{\mathrm{BOT}_{\mathrm{W}j}} = f_{i,\mathrm{W}_j} \le 0$, we have $d_i^{\mathrm{TOP}_{\mathrm{W}j}} \le d_i^{\mathrm{BOT}_{\mathrm{W}j}}$ for $i \in \mathcal{C}$, indicating that the pinch index for section $\mathrm{TOP}_{\mathrm{W}j}$ would be at least the same as the pinch index for section $\mathrm{BOT}_{\mathrm{W}j}$, hence satisfying $p^{\mathrm{TOP}_{\mathrm{W}j}} \ge p^{\mathrm{BOT}_{\mathrm{W}j}}$. Thus, we have:

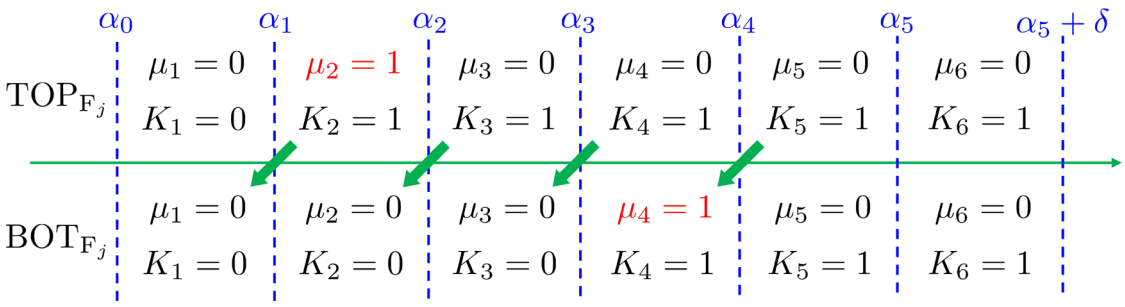

FIGURE 3 The relationship between μ_i and K_i variables for the example illustrated in Figure 2. The green arrows show how the (binary) coefficients in Equation (10) are constructed. For this example, $K_2^{\mathrm{TOP}_{\mathrm{F}j}} - K_1^{\mathrm{BOT}_{\mathrm{F}j}} = K_3^{\mathrm{TOP}_{\mathrm{F}j}} - K_2^{\mathrm{BOT}_{\mathrm{F}j}} = K_4^{\mathrm{TOP}_{\mathrm{F}j}} - K_3^{\mathrm{BOT}_{\mathrm{F}j}} = 1$. Therefore, $\mathcal{I}_{\mathrm{F}_j} = \{2,3,4\}$ according to Equation (7).

$$\sum_{i=1}^{c+1} i\mu_{i,\mathrm{BOT}_{\mathrm{W}j}} \le \sum_{i=1}^{c+1} i\mu_{i,\mathrm{TOP}_{\mathrm{W}j}} \quad \forall j = 1,\ldots,N_{\mathrm{W}}. \tag{11}$$

Similar to $\mathcal{I}_{\mathrm{F}_j}$ for feed stream F_j, we define an index set $\mathcal{I}_{\mathrm{W}_j}$ storing all indices of intervals ranging from $\max\{2, \sum_{i=1}^{c+1} i\mu_{i,\mathrm{BOT}_{\mathrm{W}j}}\}$ to $\min\{c, \sum_{i=1}^{c+1} i\mu_{i,\mathrm{TOP}_{\mathrm{W}j}}\}$. Furthermore, $\mathcal{I}_{\mathrm{W}_j}$ can also be redefined as:

$$\mathcal{I}_{\mathrm{W}_j} = \{i \in \mathcal{C} | K_i^{\mathrm{BOT}_{\mathrm{W}j}} - K_{i-1}^{\mathrm{TOP}_{\mathrm{W}j}} = 1\} \quad \forall j = 1,\ldots,N_{\mathrm{W}}. \tag{12}$$

The feasibility of separation requires the following constraint to hold for $\mathrm{TOP}_{\mathrm{W}j}$ and $\mathrm{BOT}_{\mathrm{W}j}$ for every $i \in \mathcal{I}_{\mathrm{W}_j}$[22]:

$$\gamma_{i-1}^{\mathrm{TOP}_{\mathrm{W}j}} \le \rho_{i-1,\mathrm{W}_j} \le \gamma_i^{\mathrm{BOT}_{\mathrm{W}j}} \quad \forall i \in \mathcal{I}_{\mathrm{W}_j};\ j = 1,\ldots,N_{\mathrm{W}}, \tag{13}$$

where $\{\rho_{i-1,\mathrm{W}_j}\}_{i \in \mathcal{I}_{\mathrm{W}_j}}$ satisfy Equation (14) below:

$$\sum_{m=1}^{c} \frac{\alpha_m l_{m,\mathrm{W}_j}}{\alpha_m - \rho_{i-1,\mathrm{W}_j}} = 0, \quad \text{or} \quad \sum_{m=1}^{c} \frac{\alpha_m f_{m,\mathrm{W}_j}}{\alpha_m - \rho_{i-1,\mathrm{W}_j}} = V_{\mathrm{W}_j} \quad j = 1,\ldots,N_{\mathrm{W}}. \tag{14}$$

Here, $\rho_{i-1,\mathrm{W}_j} \in (\alpha_{i-1}, \alpha_i)$. Here, $l_{m,\mathrm{W}_j} \le 0$, $f_{m,\mathrm{W}_j} \le 0$, and $V_{\mathrm{W}_j} \le 0$ correspond to the flow rate of component m in the liquid portion of the sidedraw stream, the sidedraw flow rate of component m, and the total vapor flow rate of the sidedraw, respectively. When W_j is in saturated vapor state, then l_{m,W_j} represents the hypothetical liquid sidedraw flow that is in thermodynamic equilibrium with the vapor sidedraw[22] based on Equation (1):

$$l_{m,\mathrm{W}_j} = \frac{\frac{v_{m,\mathrm{W}_j}}{\alpha_m}}{\sum_{k=1}^{c} \frac{v_{k,\mathrm{W}_j}}{\alpha_k}} \quad \forall m \in \mathcal{C}.$$

Similar to how we reformulate Equation (8) for F_j, we can rewrite Equation (13) as:

$$\begin{aligned} &(K_i^{\mathrm{BOT}_{\mathrm{W}j}} - K_{i-1}^{\mathrm{TOP}_{\mathrm{W}j}})(\gamma_i^{\mathrm{BOT}_{\mathrm{W}j}} - \rho_{i-1,\mathrm{W}_j}) \ge 0 \\ &(K_i^{\mathrm{BOT}_{\mathrm{W}j}} - K_{i-1}^{\mathrm{TOP}_{\mathrm{W}j}})(\rho_{i-1,\mathrm{W}_j} - \gamma_{i-1}^{\mathrm{TOP}_{\mathrm{W}j}}) \ge 0 \end{aligned} \quad \forall i \in \mathcal{C} \setminus \{1\};\ j = 1,\ldots,N_{\mathrm{W}}. \tag{15}$$

Furthermore, as illustrated in Figure 1, a unique feature of a sidedraw stream is that the sidedraw's liquid (resp. vapor) composition must lie on the liquid (resp. vapor) composition profile, whereas a feed stream's liquid (resp. vapor) composition may or may not lie on the liquid (resp. vapor) composition profile. The condition that the sidedraw composition must belong to the composition profile leads to the following set of constraints:

$$\begin{aligned} &K_i^{\mathrm{TOP}_{\mathrm{W}j}}(\gamma_i^{\mathrm{TOP}_{\mathrm{W}j}} - \rho_{i-1,\mathrm{W}_j}) \ge 0 \quad \forall i \in \mathcal{C} \setminus \{1\}; \\ &K_i^{\mathrm{BOT}_{\mathrm{W}j}}(\gamma_i^{\mathrm{BOT}_{\mathrm{W}j}} - \rho_{i-1,\mathrm{W}_j}) \ge 0 \quad \forall i \in \mathcal{C} \setminus \{1\}; \\ &(1 - K_i^{\mathrm{TOP}_{\mathrm{W}j}})(\gamma_i^{\mathrm{TOP}_{\mathrm{W}j}} - \rho_{i,\mathrm{W}_j}) \le 0 \quad \forall i \in \mathcal{C}; \\ &(1 - K_i^{\mathrm{BOT}_{\mathrm{W}j}})(\gamma_i^{\mathrm{BOT}_{\mathrm{W}j}} - \rho_{i,\mathrm{W}_j}) \le 0 \quad \forall i \in \mathcal{C}; \quad \forall j = 1,\ldots,N_{\mathrm{W}}. \end{aligned} \tag{16}$$

4 | IMPLEMENTATION OF MINIMUM REFLUX CALCULATION ALGORITHM

When implementing the algorithm developed in Section 3, there are two approaches to consider. The first approach is to implement Equations (4–6), (10), (15), and (16) in an optimization framework as constraints, along with the mathematical formulations of the shortcut model developed in our earlier work,[22] which includes Equations (2), (9), (14), and more. The resulting formulation is a mixed-integer nonlinear program (MINLP) for which global optimization solvers such as BARON could be utilized.[31] We pursue this approach when only the purity or recovery of the key components in product streams is specified. In this case, the MINLP determines the optimal distribution of other components in the product streams such that the reflux ratio or reboiler vapor duty requirement is minimized. To illustrate how this approach works, in Section 5.3, we present this formulation for a quaternary separation example in a two-feed, one-sidedraw column.

The second approach deals with many practical applications in which the product distributions of the MFMP column have already been adequately specified. In this case, the search for the minimum reflux ratio of the MFMP column becomes a fully algorithmic procedure that does not require solving an optimization problem. This is because the net material upward flows $\{d_i^{\mathrm{SEC}_k}\}_{i \in \mathcal{C}, k=1,\ldots,N_{\mathrm{SEC}}}$ can be readily obtained from mass balances, making the determination of pinch root location (hence $\mathcal{I}_{\mathrm{F}}$ and $\mathcal{I}_{\mathrm{W}}$ sets) completely deterministic for every feed and sidedraw stream. Therefore, we can run a simple algorithmic procedure, as shown in Algorithms 1–3, to identify the true minimum reboiler vapor duty requirement (or equivalently, the minimum reflux ratio since all product flows are fixed). Specifically, as discussed in detail in our previous work,[22] at minimum reflux condition, one of the feed or side-draw streams essentially "controls" the separation. Accordingly, while the feasibility constraints (Equation 8 or 13) associated with feed and/or sidedraw streams continue to hold, the feasibility constraints associated with the controlling feed or sidedraw stream will become binding (i.e., satisfied as equalities). Thus, the idea behind Algorithms 1 through 3 is to scrutinize all feed and sidedraw streams, assuming that each of them might be "controlling" the separation at minimum reflux, and determine whether feasibility constraints are met for the rest of the feed and sidedraw streams. Overall, the true reboiler vapor duty (resp. minimum reflux ratio) corresponds to the lowest reboiler vapor duty (resp. lowest reflux ratio) at which all feasibility constraints are satisfied.

5 | CASE STUDIES

In this section, we examine a few ternary and quaternary separation examples that illustrate the accuracy and effectiveness of our minimum reflux calculation methods while providing new and valuable insights into the minimum reflux behavior of an MFMP column.

Algorithm 1 `Vrebmin`: **Algorithm for determining the minimum reboiler vapor duty requirement of an MFMP column knowing the flow rates and compositions of feed and product streams. The minimum reflux ratio $R_{\min}$ can be readily calculated from vapor balances once $V_{\text{reb,min}}$ is obtained, since all feed and product flow rates are specified.**

input : $\mathcal{C}$, N_{F}, N_{W}, N_{SEC}, $\{f_{i,\text{F}_j}\}_{j=1}^{N_{\text{F}}}$, $\{l_{i,\text{F}_j}\}_{j=1}^{N_{\text{F}}}$, $\{f_{i,\text{W}_j}\}_{j=1}^{N_{\text{W}}}$, $\{l_{i,\text{W}_j}\}_{j=1}^{N_{\text{W}}}$, $d_i^{\text{SEC}_1}$ for every component $i \in \mathcal{C}$
output: minimum reboiler vapor duty $V_{\text{reb,min}}$
initialize: An empty list $\{V_{\text{reb}}\}$ storing candidate minimum reboiler vapor duty values

begin
  Calculate $\{d_i^{\text{SEC}_k}\}_{i\in\mathcal{C};\, k=2,\ldots,N_{\text{SEC}}}$ from inter-column section material balances: $d_i^{\text{SEC}_k} = d_i^{\text{SEC}_{k-1}} - f_{i,\text{F}_j}$ if SEC_k and SEC_{k-1} are connected by a feed stream F_j, and $d_i^{\text{SEC}_k} = d_i^{\text{SEC}_{k-1}} - f_{i,\text{W}_j}$ if SEC_k and SEC_{k-1} are connected by a sidedraw stream W_j;
  Determine pinch root $\{\gamma_p^{\text{SEC}_k}\}_{k=1,\ldots,N_{\text{SEC}}}$ locations from Equation (3) and other edge cases, then obtain $\{\mu_i^{\text{SEC}_k}\}_{i\in\mathcal{C},k=1,\ldots,N_{\text{SEC}}}$ and $\{K_i^{\text{SEC}_k}\}_{i\in\mathcal{C},k=1,\ldots,N_{\text{SEC}}}$;
  Determine index sets $\{\mathscr{I}_{\text{F}_j}\}_{j=1}^{N_{\text{F}}}$ and $\{\mathscr{I}_{\text{W}_j}\}_{j=1}^{N_{\text{W}}}$ from Equations (7) and (12);
  Solve Equations (9) and (14) to obtain $\{\rho_{i-1,\text{F}_j}\}_{i\in\mathcal{C}\setminus\{1\};\, j=1,\ldots,N_{\text{F}}}$ and $\{\rho_{i-1,\text{W}_j}\}_{i\in\mathcal{C}\setminus\{1\};\, j=1,\ldots,N_{\text{W}}}$ roots, respectively;
  for $j \leftarrow 1$ **to** N_{W} **do**
    Add $V_{\text{reb},\text{W}_j} = \texttt{sidedrawFeasible}(j, \{K_i^{\text{TOP}_{\text{W}_j}}\}_i)$ into the list $\{V_{\text{reb}}\}$ and continue;
    if $\mathscr{I}_{\text{W}_j} = \emptyset$ **then** Skip and go to the next j **else** Continue;
    for $i \in \mathscr{I}_{\text{W}_j}$ **do**
      Substitute $\gamma_{i-1}^{\text{TOP}_{\text{W}_j}} \leftarrow \rho_{i-1,\text{W}_j}$ into Equation (2) to obtain $V^{\text{TOP}_{\text{W}_j}}$;
      Add $V_{\text{reb},\text{W}_j} = \texttt{getVreb}(\text{TOP}_{\text{W}j}, V^{\text{TOP}_{\text{W}_j}})$ into the list $\{V_{\text{reb}}\}$;
    end
  end
  for $j \leftarrow 1$ **to** N_{F} **do**
    if $\mathscr{I}_{\text{F}_j} = \emptyset$ **then** Skip and go to the next j **else** Continue;
    for $i \in \mathscr{I}_{\text{F}_j}$ **do**
      Substitute $\gamma_i^{\text{TOP}_{\text{F}_j}} \leftarrow \rho_{i-1,\text{F}_j}$ into Equation (2) to obtain $V^{\text{TOP}_{\text{F}_j}}$;
      Add $V_{\text{reb},\text{F}_j} = \texttt{getVreb}(\text{TOP}_{\text{F}j}, V^{\text{TOP}_{\text{F}_j}})$ into the list $\{V_{\text{reb}}\}$;
    end
  end
  $V_{\text{reb,min}} = \min\{V_{\text{reb}}\}$
end

5.1 | Example 1: Two-feed distillation column

In the first example, we examine a two-feed distillation column shown in Figure 4 separating a ternary mixture of n-hexane (Component 3), n-heptane (Component 2), and n-octane (Component 1). Two-feed columns are common in extractive distillation applications. Furthermore, as recently discovered by Madenoor Ramapriya et al.,[32] a large energy saving can potentially be realized when two feed streams are introduced at two different locations of the column compared to premixing them to form a single feed stream.

The relative volatility of each component with respect to n-octane at atmospheric pressure is estimated from Aspen Plus to be $(\alpha_3,\alpha_2,\alpha_1) = (5.1168, 2.25, 1)$. To establish a common basis for comparison, we ensure constant relative volatility and constant molar overflow assumptions by appropriately modifying the property parameters in Aspen Plus listed under PLXANT and DHVLDP.[33] The IDEAL thermodynamic package is used. This column produces a distillate product with a total flow rate of 52.476 mol/s containing 95 mol% of n-hexane, 5 mol% of n-heptane, and a negligible amount of n-octane. Thus, the bottom product has a flow rate of 147.524 mol/s containing 0.1 mol% of n-hexane, 45.671 mol% of n-heptane, and 54.229 mol% of n-octane.

We consider two scenarios in Example 1. In the first scenario, the upper feed F_1 in the MFMP column is a saturated liquid stream containing 30 mol/s of n-hexane, 60 mol/s of n-heptane, and 10 mol/s of n-octane. The lower feed F_2 is also a saturated liquid stream but with 20 mol/s of n-hexane, 10 mol/s of n-heptane, and 70 mol/s of n-octane. Clearly, F_2 is less volatile (i.e., "heavier") than F_1 and thus has a higher bubble point temperature. Since the feed and product

Algorithm 2 `getVreb`**: Algorithm for checking the feasibility of separation and returning the candidate reboiler vapor duty value.**

input : column section s and its section vapor flow V^{SEC_s}
output: candidate reboiler vapor duty value

begin
  for $k \leftarrow s-1$ **to** 1 **do**
    Calculate V^{SEC_k} from $V^{\mathrm{SEC}_{k+1}}$ via vapor balances:
    $V^{\mathrm{SEC}_k} = V^{\mathrm{SEC}_{k+1}} + \sum_{i\in\mathscr{C}}(f_{i,\mathrm{F}_j} - l_{i,\mathrm{F}_j})$ if SEC_k and SEC_{k+1} are connected by feed stream F_j, and
    $V^{\mathrm{SEC}_k} = V^{\mathrm{SEC}_{k+1}} + \sum_{i\in\mathscr{C}}(f_{i,\mathrm{W}_j} - l_{i,\mathrm{W}_j})$ if SEC_k and SEC_{k+1} are connected by sidedraw stream W_j;
    Determine $\{\gamma_r^{\mathrm{SEC}_k}\}_{r\in\mathscr{C}}$ from Equation (2) using V^{SEC_k};
    if the feasibility constraints (Equations (8), (13), (16)) associated with SEC_k are satisfied **then** Continue **else return** `null`;
  end
  for $k \leftarrow s+1$ **to** N_{SEC} **do**
    Calculate V^{SEC_k} from $V^{\mathrm{SEC}_{k-1}}$ via vapor balances;
    Determine $\{\gamma_r^{\mathrm{SEC}_k}\}_{r\in\mathscr{C}}$ from Equation (2) using V^{SEC_k};
    if the feasibility constraints (Equations (8), (13), (16)) associated with SEC_k are satisfied **then** Continue **else return** `null`;
  end
  return $V^{\mathrm{SEC}_{N_{\mathrm{SEC}}}}$.
end

Algorithm 3 `sidedrawFeasible`**: Algorithm for returning candidate reboiler vapor duty value assuming that the minimum reflux is "controlled" by a sidedraw.**

input : sidedraw stream index j and index set $\{K_i^{\mathrm{TOP}_{\mathrm{W}_j}}\}_i$
output: candidate reboiler vapor duty value
initialize: An empty list $\{V_{\mathrm{reb},\mathrm{W}_j}\}$ storing candidate minimum reboiler vapor duty values

begin
  Determine all $\{\rho_{i-1,\mathrm{W}_j}\}_{i\in\mathscr{C}\setminus\{1\}}$ roots from Equation (14);
  for $m \leftarrow 1$ **to** c **do**
    if $K_m^{\mathrm{TOP}_{\mathrm{W}_j}} = 0$ **then**
      Substitute $\gamma_m^{\mathrm{TOP}_{\mathrm{W}_j}} \leftarrow \rho_{m,\mathrm{W}_j}$ into Equation (2) to obtain $V^{\mathrm{TOP}_{\mathrm{W}_j}}$; Add $V_{\mathrm{reb},m} = \mathtt{getVreb}(\mathrm{TOP}_{\mathrm{W}_j}, V^{\mathrm{TOP}_{\mathrm{W}_j}})$ into the list $\{V_{\mathrm{reb},\mathrm{W}_j}\}$;
    else
      Substitute $\gamma_m^{\mathrm{TOP}_{\mathrm{W}_j}} \leftarrow \rho_{m-1,\mathrm{W}_j}$ into Equation (2) to obtain $V^{\mathrm{TOP}_{\mathrm{W}_j}}$; Add $V_{\mathrm{reb},m} = \mathtt{getVreb}(\mathrm{TOP}_{\mathrm{W}_j}, V^{\mathrm{TOP}_{\mathrm{W}_j}})$ into the list $\{V_{\mathrm{reb},\mathrm{W}_j}\}$;
  end
  return $V^{\mathrm{SEC}_{N_{\mathrm{SEC}}}} \leftarrow \min\{V_{\mathrm{reb},\mathrm{W}_j}\}$.
end

specifications are given, we determine that $\mathcal{I}_{\mathrm{F}_1} = \{2,3\}$ and $\mathcal{I}_{\mathrm{F}_2} = \{3\}$ based on our earlier discussion in Section 2. Substituting these index sets into Algorithms 1 through 3, we obtain that the minimum reflux ratio $R_{\min} = 2.162$ and the corresponding minimum reboiler vapor duty is $V_{\mathrm{reb,min}} = 165.95$ mol/s. The minimum reflux condition occurs when the upper feed F_1 "controls" the separation, in which

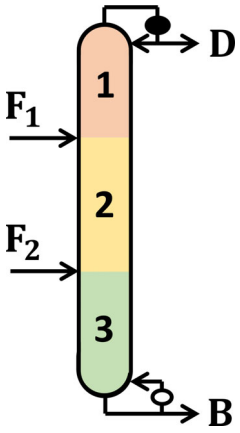

FIGURE 4 A two-feed column with no side-draw product stream.

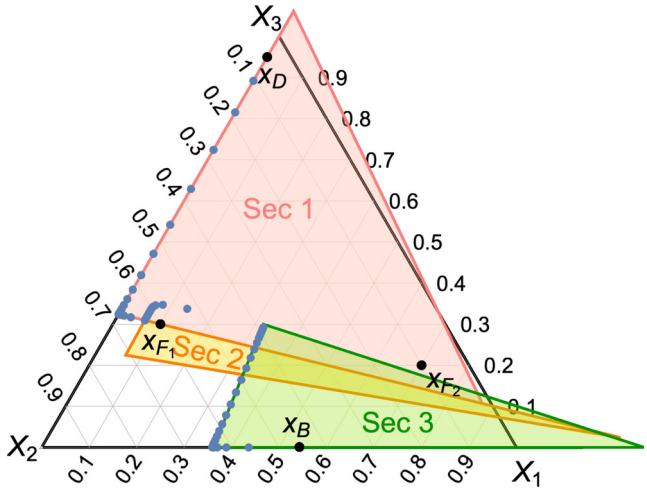

FIGURE 5 The pinch simplices at the minimum reflux condition obtained using Algorithms 1 through 3. Hereafter, X_1, X_2, X_3 represent pure n-octane, n-heptane, and n-hexane, respectively. The colors of the pinch simplices match those in Figure 4. The blue dots are the actual liquid composition profile of this two-feed column simulated in Aspen Plus as a RadFrac column. By setting up appropriate `Design Specs` in Aspen Plus to simulate the MFMP containing 150 equilibrium stages, we obtain a minimum reflux ratio of $R_{\min} = 2.145$ from Aspen Plus. The exact pinches compositions in SEC_1 through SEC_3 are Z_2 (associated with pinch root $\gamma_p^{SEC_1} = \gamma_2^{SEC_1} \in (\alpha_1, \alpha_2)$), Z_3 (associated with pinch root $\gamma_p^{SEC_2} = \gamma_3^{SEC_2} \in (\alpha_2, \alpha_3)$), and Z_3 ($\gamma_p^{SEC_3} = \gamma_3^{SEC_3} \in (\alpha_3, \alpha_3 + \delta)$), respectively. Therefore, $\mu_2^{SEC_1} = \mu_3^{SEC_2} = \mu_4^{SEC_3} = 1$.

Equation (8) associated with $i = 3$ in $\mathcal{I}_{F_1}$ becomes the binding constraint ($\gamma_3^{TOP_{F1}} = \gamma_2^{BOT_{F1}} = \rho_{2,F_2}$).

For this ternary separation, we can visualize its minimum reflux condition by constructing the pinch simplicies in Figure 5 based on our previous work.[22] We observe that the pinch simplices associated with SEC_1 and SEC_2 share a common boundary, where F_1 stream composition $\mathbf{x}_{F_1}$ also lies. This means the two boundaries of the pinch simplices satisfy $z_3^{TOP_{F1}}(\mathbf{x}_{F_1}) = z_2^{BOT_{F1}}(\mathbf{x}_{F_1}) = 0$, which implies $\gamma_3^{TOP_{F1}} = \gamma_2^{BOT_{F1}} = \rho_{2,F_2}$ (see Figure 6 for illustration of pinch simplex; readers may refer to our previous work[22] for detailed explanation). In other words, the geometric interpretation of feasible separation is that the pinch simplices of any two adjacent column sections must be connected, and the minimum reflux condition occurs when the pinch simplices sandwiching the controlling feed or sidedraw stream share a common face. If the reflux ratio is further reduced, these two simplices will no longer be connected, or $z_3^{TOP_{F1}}(\mathbf{x}_{F_1}) < 0$, and $z_2^{BOT_{F1}}(\mathbf{x}_{F_1}) < 0$. This indicates that $\gamma_3^{TOP_{F1}} < \rho_{2,F_1}$ and $\gamma_2^{BOT_{F1}} > \rho_{2,F_1}$, hence violating the feasibility constraint of Equation (8) for feed F_1. Therefore, $R_{\min} = 2.162$ is indeed the minimum reflux ratio.

We validate the minimum reflux ratio obtained from our shortcut method using rigorous Aspen Plus simulation. Each column section contains 50 equilibrium stages, much larger than what is needed for this paraffin separation task. This is to ensure that the true minimum reflux condition is achieved. It turns out that the minimum reflux ratio obtained from our shortcut method is less than 1% different compared to the true minimum reflux ratio ($R_{\min} = 2.145$) obtained from rigorous Aspen Plus simulation. Also, the liquid composition profile inside this two-feed column at minimum reflux, as shown in Figure 7, exactly follows the behavior of the liquid composition trajectory bundle of a pinch simplex (see Figure 6). For more details, readers are directed to review Sections 3.4 and 4.2 of Jiang et al.[22] Specifically, since the distillate product is free of n-octane, the liquid composition profile $\mathbf{x}_n$ (where stage number n is numbered from top to bottom) starting from the distillate product ($n = 0$) must lie on the hyperplane $z_1^{SEC_1}(\mathbf{x}) = 0$ until it reaches a (saddle) pinch,[34,35] which corresponds to vertex Z_2 of the pinch simplex and lies inside SEC_1. Below this pinch, the liquid composition profile continues along the hyperplane $z_3^{SEC_1}(\mathbf{x}) = 0$ until it reaches the lower end of SEC_1, which is connected to the top of SEC_2 (see Figure 7). It turns out this is where the pinch zone lies for SEC_2. Since this pinch is an unstable node when moving downward along the column, the liquid composition profile moves away from the pinch until it reaches the top of SEC_3. Again, the pinch zone of SEC_3 is located at the top of the section, from which the composition profile follows its trajectory inside the pinch simplex and heads toward the stable node (Z_1) until it reaches the bottom product composition. It is worth noting that, while the n-hexane composition is small in the bottom product (0.1 mol%), it is not negligible. Thus, although the liquid composition profile inside SEC_3 may appear to be approaching the saddle point pinch, it never actually reaches the saddle pinch, which can be seen from Figure 7.

Next, using the same two-feed column example, we will examine the prevailing modeling heuristics that (1) an MFMP column can be decomposed into a series of simple columns with exactly one feed and two products, and (2) the actual minimum reflux ratio of the original MFMP column is simply the largest minimum reflux ratio value determined for all decomposed simple columns (which can be determined by applying the classic Underwood method[36,37]). According to column decomposition, the two-feed column of Figure 4 is modeled as two simple columns, with one having F_1 as the feed stream and consisting of SEC_1 and SEC_2, whereas the other with F_2 as the feed stream and consisting of SEC_2 and SEC_3. In this case, it turns out that the largest minimum reflux ratio of the two decomposed simple

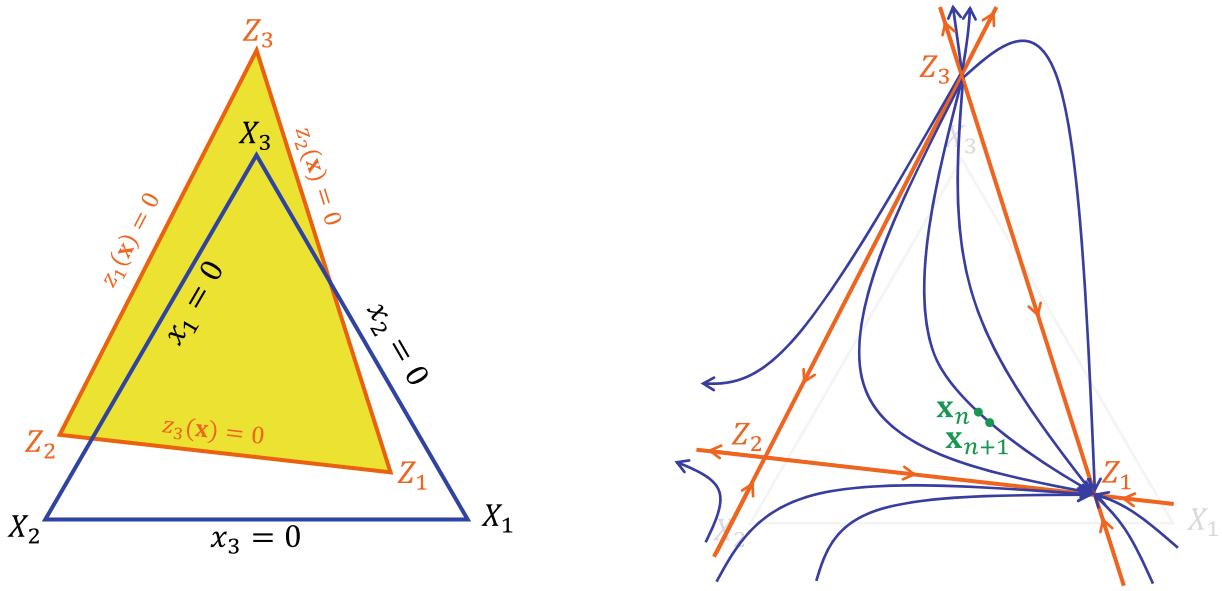

FIGURE 6 An illustration of a pinch simplex constructed for a column section and liquid composition trajectory bundle. The pinch simplex boundary $z_i(\mathbf{x}) = 0$ is associated with the root γ_i (see Table 1 of Jiang et al.[22] for explanation). And possible pinch compositions are given by the vertices of the pinch simplex, Z_i. The arrows indicate the direction of liquid composition evolution as we move downward from the top of the column section.

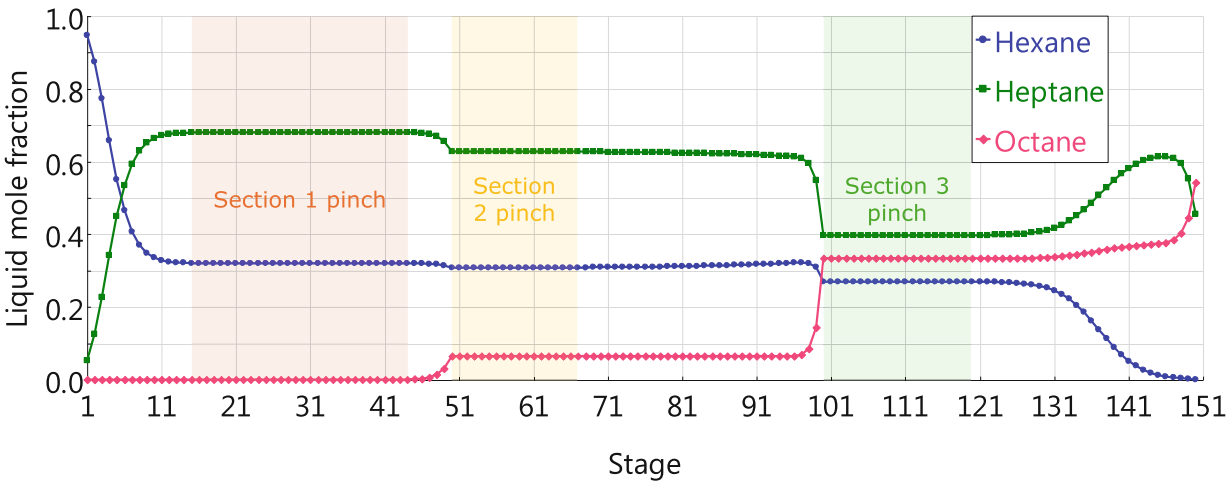

FIGURE 7 The liquid composition profile retrieved from Aspen Plus at the true minimum reflux ratio of $R_{min} = 2.145$. Based on the classifications in Lucia et al.,[34,35] the pinch in SEC_1 is a saddle point and is located inside the column section, whereas the pinches in SEC_2 and SEC_3 are both unstable nodes and are located at the top of their column sections. Note that the colors of these pinch zones match with their pinch simplices drawn in Figure 5.

columns is identified as 2.618, which is significantly higher than the true minimum reflux ratio. In other words, the column decomposition approach overestimates the true minimum reflux in this example.

Now, we consider the second scenario where the locations of the two feed streams are switched. In other words, the upper feed F_1 is less volatile than the lower feed F_2. The distillate and bottoms product specifications remain unchanged. Using Algorithms 1through 3, we determine that the minimum reflux ratio of this new arrangement is $R_{min} = 1.683$, at which the lower feed F_2 controls the separation. This can be visualized from the pinch simplex diagram of Figure 8, where sections TOP_{F2} (i.e., SEC_2) and BOT_{F2} (i.e., SEC_3) share a common boundary, indicating that $\gamma_3^{TOP_{F2}} = \gamma_2^{BOT_{F2}} = \rho_{2,F_2}$ is the binding constraint. Rigorous Aspen Plus simulation shows that the true minimum reflux ratio is 1.738. Thus, our shortcut model gives an accurate estimation of the minimum reflux ratio with a 3% relative difference compared to the true minimum reflux ratio. Furthermore, if we adopt the column decomposition method, we would end up with a "minimum reflux ratio" that is as high as 19.714, which is almost 11.3 times as

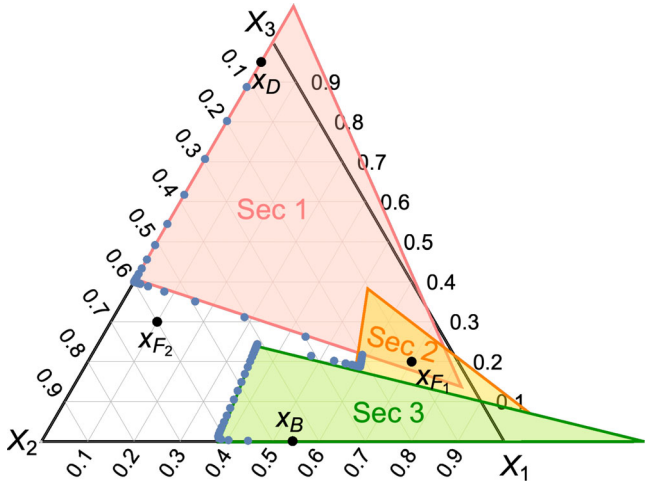

FIGURE 8 For the case where the upper feed is less volatile than the lower feed, the pinch simplex diagram at the calculated minimum reflux ratio of $R_{min} = 1.683$. The blue dots indicate the liquid composition profile at $R = 1.738$, which is the minimum reflux ratio predicted by rigorous Aspen Plus simulation.

large as the true minimum reflux ratio! Clearly, designing or operating the MFMP column based on an incorrect minimum reflux ratio will lead to tremendous capital and operating costs.

By examining the two scenarios, we find that the optimal feed arrangement does not necessarily follow any particular pattern based on its temperature. Intuitively, one might think that, to reduce energy consumption (i.e., reflux ratio), feed streams should be placed according to their temperatures. Specifically, a common belief is that a high-temperature feed should be placed closer to the bottom of the column than a low-temperature feed. However, it turns out that, despite achieving the same product flow rates and purities, the minimum reflux ratio in the first scenario ($R_{min} = 2.162$) is much higher than that in the second scenario ($R_{min} = 1.683$)! This finding matches the observation first made by Levy and Doherty.[38] Here, we provide the first systematic analysis of the contradictions to the common belief that a high-temperature feed should be placed below a low-temperature feed. Practitioners should examine carefully the optimal feed arrangement when designing their columns. In this regard, our shortcut model and minimum reflux calculation method allow practitioners to obtain a quick and reliable screening of the optimal feed arrangement.

5.2 | Example 2: A one-feed, two-side-product column

In this example, we study a distillation column separating a ternary mixture of n-hexane, n-heptane, and n-octane with one feed stream and two side-draw product streams, as shown in Figure 9. When there is only one feed stream and both side-draw products are withdrawn as saturated liquids, there is a common belief in the literature (e.g., Sugie and Lu,[39] Glinos and Malone[40]) that F_1 will always be "controlling" the separation at minimum reflux.

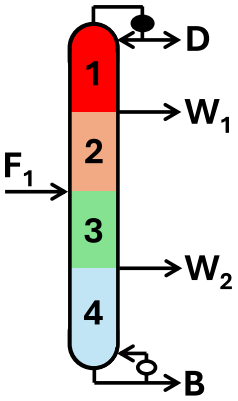

FIGURE 9 A one-feed column with two side-draw streams is considered in Example 2. The colors of the pinch simplices match those in Figure 9.

This assumption originates from the observation of the McCabe-Thiele diagram for binary distillation with saturated liquid sidedraws, where the operating lines for sections above F_1 continuously decreases from the top of the column to F_1, and the operating lines for sections below F_1 continuously increases from the bottom of the column to F_1.

To verify if this result can be generalized to multicomponent distillation, we present this example where F_1 is a saturated liquid stream containing 30 mol/s of n-hexane (Component 3), 40 mol/s of n-heptane (Component 2), and 30 mol/s of n-octane (Component 1). The distillate stream contains 24 mol/s of n-hexane, 6 mol/s of n-heptane, and a negligible amount of n-octane, whereas the bottoms product contains 20 mol/s of n-octane and no n-hexane or n-heptane. The upper side draw W_1, which is located above F_1, is a saturated liquid stream with 6 mol/s of n-hexane and 24 mol/s of n-heptane. The lower side draw W_2 is also a saturated liquid stream with 10 mol/s of n-heptane and 10 mol/s of n-octane. Once $\{d_i^{SEC_k}\}_{i,k}$ are determined, we determine that $\mathcal{I}_{W_1} = \{2\}, \mathcal{I}_{F_1} = \{2,3\}, \mathcal{I}_{W_2} = \{2,3\}$.

By applying Algorithms 1 through 3, we determine that the minimum reflux ratio is $R_{min} = 2.693$, which is less than 1% different compared to the rigorous Aspen Plus simulation minimum reflux ratio result of 2.668. From the minimum reflux pinch simplex diagram of Figure 10, we can see that sidedraw W_1 actually controls the separation at minimum reflux. Specifically, the minimum reflux occurs when $z_2^{TOP_{W1}}(\mathbf{x}_{W_1}) = z_2^{BOT_{W1}}(\mathbf{x}_{W_1}) = 0$, indicating that $\gamma_3^{TOP_{W1}} = \gamma_3^{BOT_{W1}} = \rho_{2,W_1}$. This is a consequence of Equation (16), which requires that the sidedraw composition $\mathbf{x}_{W_1}$ must lie on the liquid composition profile, and thus must not reside outside of the pinch simplices associated with SEC_1 and SEC_2. If the reflux ratio drops below this minimum threshold, the sidedraw composition $\mathbf{x}_{W_1}$ no longer resides within the pinch simplices, as their boundaries $z_3^{TOP_{W1}}(\mathbf{x}) = 0$ and $z_3^{BOT_{W1}}(\mathbf{x}) = 0$ would move toward X_3 (pure n-hexane), hence violating Equation (13) see Figure 11.

Now, to see what happens when we insist F_1 to control the separation at minimum reflux, we relax the feasibility constraints in Algorithms 1 through 3by ignoring Equation (16). This gives a "minimum reflux ratio" of 2.533, which is lower than the true minimum reflux ratio. As a result, we have provided a counterexample to the common

belief that the feed stream always controls the minimum reflux operation when sidedraws are taken as saturated liquid streams. Without incorporating the constraints related to sidedraws, one may completely ignore the possibility that a sidedraw could control the separation at minimum reflux and thus will obtain an incorrect minimum reflux ratio value that causes infeasible separation. To the best of our knowledge, this work is the first to derive these sidedraw-related constraints and incorporate them into an algorithmic framework to calculate the true minimum reflux ratio for MFMP columns. Furthermore, we remark that our proposed minimum reflux calculation method is a generalized framework that is not limited to single-feed columns in saturated liquid sidedraws.

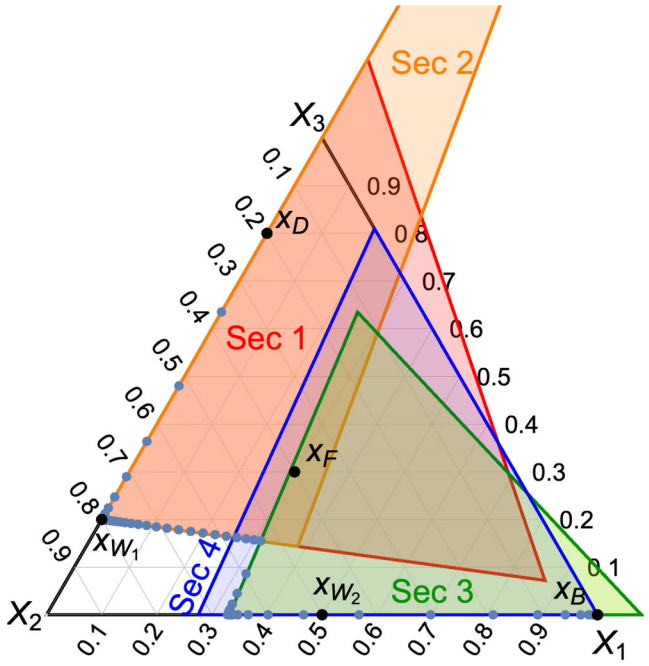

FIGURE 10 The pinch simplex diagram for a one-feed, two-side-product column example at minimum reflux ($R_{min} = 2.693$), along with the liquid composition profile at the minimum reflux of $R_{min} = 2.668$ identified by Aspen Plus (also see Figure 11). The exact pinches compositions in SEC_1 through SEC_4 are Z_2 (associated with pinch root $\gamma_p^{SEC_1} = \gamma_2^{SEC_1} \in (\alpha_1, \alpha_2)$), Z_2 (associated with pinch root $\gamma_p^{SEC_2} = \gamma_2^{SEC_2} \in (\alpha_1, \alpha_2)$), Z_2 (associated with pinch root $\gamma_p^{SEC_3} = \gamma_2^{SEC_3} \in (\alpha_2, \alpha_3)$), and Z_1 ($\gamma_p^{SEC_4} = \gamma_1^{SEC_4} \in (\alpha_1, \alpha_2)$), respectively. Therefore, $\mu_2^{SEC_1} = \mu_2^{SEC_2} = \mu_3^{SEC_3} = \mu_2^{SEC_4} = 1$.

5.3 | Example 3: A two-feed, one-side-product column

In the third example, we study an MFMP column drawn in Figure 12A that separates n-hexane (Component A or 4), n-heptane (Component B or 3), n-octane (Component C or 2), and n-nonane (Component D or 1). The relative volatilities with respect to nonane are $(\alpha_4, \alpha_3, \alpha_2, \alpha_1) = (12.332, 5.361, 2.300, 1)$. Such an MFMP column is very common in multicomponent distillation configurations,[5] and it can be obtained by consolidating two simple columns and merging the common product stream BC into a sidedraw stream. For this MFMP column, the upper feed F_1 (ABC) is a saturated vapor stream with 30 mol/s of n-hexane (Component A), 30 mol/s of n-heptane (Component B), and 40 mol/s of n-octane (Component C), whereas the lower feed F_2 (BCD) is a saturated liquid stream with 40 mol/s of n-heptane, 30 mol/s of n-octane, and 30 mol/s of n-nonane (Component D). The sidedraw W_1 (BC) is in a saturated liquid state. In terms of product specifications, we require that the most volatile component A must be completely recovered in the distillate stream, whereas the least volatile component D must be completely recovered in the bottoms product. The distributions of intermediate components B and C in product streams, on the other hand, are flexible. Depending on what the distributions are, component B in SEC_2 and component C in SEC_3 could have either net material upward or downward flow. For instance, when component B in

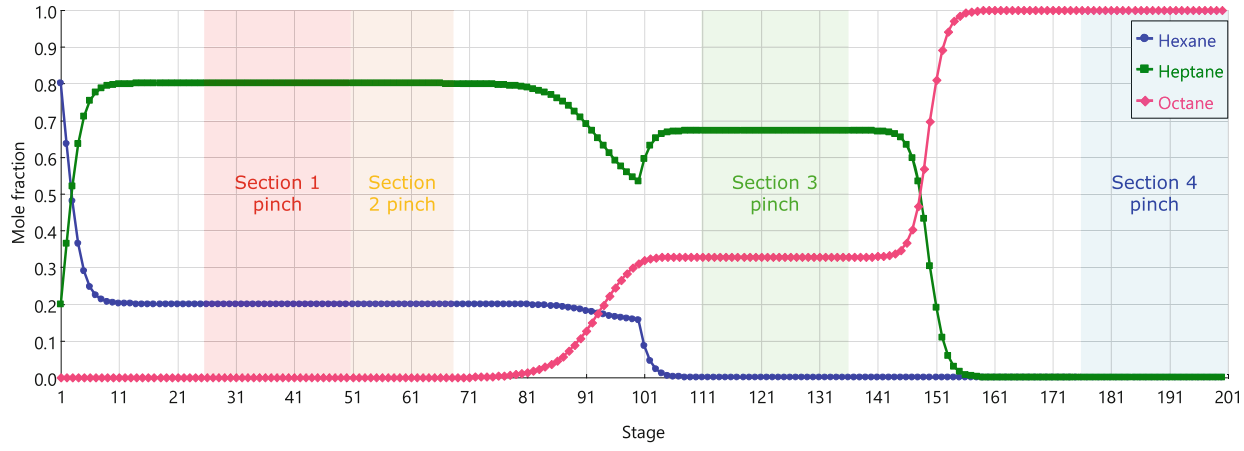

FIGURE 11 The liquid composition profile retrieved from Aspen Plus at the true minimum reflux ratio $R_{min} = 2.668$. Each of the four column sections is given 50 equilibrium stages. The pinch zones in SEC_1 through SEC_4 are located, respectively, at the bottom, at the top, within, and at the bottom of their corresponding column sections. Note that the colors of these pinch zones match with their pinch simplices drawn in Figure 10.

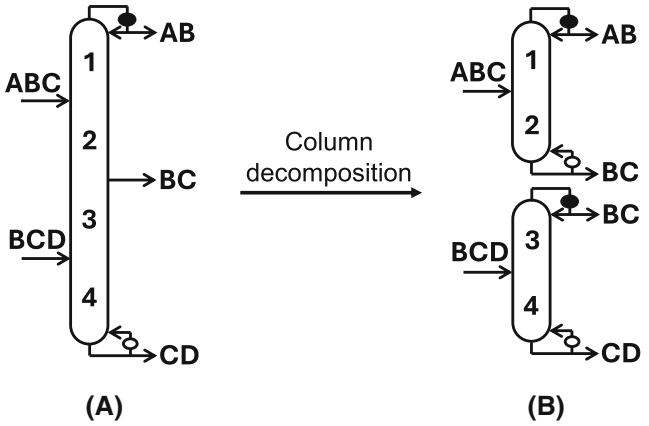

FIGURE 12 (A) An MFMP column for quaternary separation; (B) the decomposed version of (A).

SEC_2 has net material upward flow ($d_3^{SEC_2} > 0$), some of component B coming from the lower feed F_2 will travel all the way to the top of the column and be produced as distillate. Because of this, the pinch root $\gamma_p^{SEC_2} = \gamma_3^{SEC_2}$ may lie in either (α_2,α_3) or (α_3,α_4). Similarly, the pinch root $\gamma_p^{SEC_3} = \gamma_2^{SEC_3}$ may lie in either (α_1,α_2) or (α_2,α_3). As a result, we only need one binary variable, $\mu_3^{SEC_2}$, to indicate whether $\gamma_p^{SEC_2}$ lies in (α_2,α_3) or not. Similarly, we also only need one binary variable, $\mu_2^{SEC_3}$, to indicate whether $\gamma_p^{SEC_3}$ lies in (α_1,α_2) or not.

Furthermore, since $\gamma_3^{SEC_2} \in (\alpha_2,\alpha_4)$ and $\gamma_2^{SEC_3} \in (\alpha_1,\alpha_3)$, singularity issue might arise when implementing Equation (2) in the optimization model when pinch root $\gamma_3^{SEC_2}$ takes the value α_3 and/or when pinch root $\gamma_2^{SEC_3}$ takes the value α_2. To avoid the singularity issue, we reformulate Equation (2) by multiplying both sides of it by the bound factor (e.g., $(\alpha_3 - \gamma_3^{SEC_2})$ for V^{SEC_2}) followed by performing partial fraction decomposition. For example, the V^{SEC_2} expression can be reformulated as:

$$V^{SEC_2}(\alpha_3 - \gamma_3^{SEC_2}) = (\alpha_3 - \gamma_3^{SEC_2})\frac{\alpha_2 d_2^{SEC_2}}{\alpha_2 - \gamma_3^{SEC_2}} + \alpha_3 d_3^{SEC_2}$$
$$= \alpha_2 d_2^{SEC_2} + (\alpha_3 - \alpha_2)\frac{\alpha_2 d_2^{SEC_2}}{\alpha_2 - \gamma_3^{SEC_2}} + \alpha_3 d_3^{SEC_2},$$

which we note that $d_1^{SEC_2} = d_4^{SEC_2} = 0$ because n-hexane is completely recovered in the distillate stream and n-nonane is completely recovered in the bottoms stream, as shown in Figure 12. Similarly, we can reformulate the V^{SEC_3} expression using this technique. With this, we can safely bound $\gamma_3^{SEC_2} \in (\alpha_2,\alpha_4)$ and $\gamma_2^{SEC_3} \in (\alpha_1,\alpha_3)$ witout concerning about the singularity issue. In Online Appendix C, we provide all the equations and constraints needed to determine the optimal distribution of intermediate components to minimize the reboiler vapor duty requirement (i.e., V^{SEC_4}) for this MFMP column. The resulting optimization model, which is a mixed-integer nonlinear program (MINLP), is solved to global optimality within 15 CPU seconds in a Dell Precision 7865 workstation (equipped with 128 GB RAM and AMD Ryzen Threadripper PRO 5975WX 32-Cores 3.6 GHz processor) using global solver BARON 24.3[31] via GAMS 46.5. In Online Appendix C, we provide the complete MINLP formulation implemented in GAMS. The lowest possible minimum reboiler vapor duty $V_{reb,min}$ (i.e., minimum vapor duty in SEC_4) is determined to be 71.87 mol/s. And the corresponding optimal product distributions are summarized in Table 1.

TABLE 1 Optimal distributions of n-hexane, n-heptane, n-octane, and n-nonane in all product streams at $V_{reb,min} = 71.87$ mol/s.

Stream	Label in Figure 12A	Flow rate of component A, B, C, D (mol/s)
Distillate	AB	30, 14.23, 0, 0
Sidedraw	BC	0, 55.77, 48.94, 0
Bottoms	CD	0, 0, 21.06, 30

Note: One can determine that $d_4^{SEC_2} = 0$ and $d_3^{SEC_2} = -15.77$ mol/s < 0, and thus $\mu_4^{SEC_2} = 1$. Meanwhile, $d_2^{SEC_3} = 8.94$ mol/s > 0 and $d_1^{SEC_3} = 0$, and thus $\mu_2^{SEC_3} = 1$.

We verify this result by performing exhaustive sensitivity analysis using Aspen Plus. The lowest reboiler vapor duty requirement that satisfies product requirements is found to be 77.9 mol/s, which is within 8.3% relative difference compared to the MINLP result. The associated n-heptane and n-octane flow rates in product streams also match very well with the results shown in Table 1. This validates the accuracy and computational efficiency of the global optimization framework based on the shortcut model. Moreover, we remark that the global optimization algorithm does more than just finding the minimum energy requirement of an MFMP column and its corresponding product distributions. For example, there has been a lingering question among the distillation community of whether all n-heptane can be recovered from the distillate product in this MFMP column. We can easily answer questions like this by modifying the relevant variable bounds and/or by adding/deactivating related constraints in the MINLP formulation. In this case, by introducing a new constraint $d_3^{SEC_1} = f_{3,F_1} + f_{3,F_2}$ into the MINLP formulation, the resulting optimization problem turns out to be infeasible. Thus, we conclude that it is impossible to recover all the n-heptane in the distillate product. Rigorous Aspen Plus simulation also confirms that some n-heptane is always drawn from the side draw, no matter how much vapor is generated at the reboiler.

Lastly, using this MFMP column as an example, we illustrate why the column decomposition method shown in Figure 12 fails to calculate the true minimum reflux ratio. The product flow rates and compositions in this example have already been specified and are listed in Table 2. The minimum reflux ratio (which is also achieved when reboiler vapor duty is minimized as product flow rates are fixed) can be calculated using Algorithm 1 or the approach. In particular, it is worth mentioning that the resulting optimization program is solved to global optimality instantaneously during the preprocessing step. Both approaches give the same minimum reflux ratio of $R_{min} = 2.002$, which is only 0.1% different from the minimum reflux ratio of 2.000 predicted by the Aspen Plus simulation. Furthermore, this is achieved when the side-draw BC controls the minimum reflux condition.

TABLE 2 Component molar flow rates (arranged as n-hexane, n-heptane, n-octane, and lastly n-nonane) of all product streams.

Stream	Label in Figure 12A	Flow rate of component A, B, C, D (mol/s)
Distillate	AB	30, 40, 0, 0
Sidedraw	BC	0, 30, 40, 0
Bottoms	CD	0, 0, 30, 30

Meanwhile, the column decomposition method, which calculates the minimum reflux ratio of two simple columns as shown in Figure 12B using the classic Underwood method, yields a "minimum reflux ratio" of 1.806, which is significantly lower than the true minimum reflux ratio. In other words, if the column operates at $R = 1.806$, the desired separation can never be achieved.

There are two main reasons why the column decomposition technique fails in this example. First, from Table 2, one can determine that the component distillate flow for n-heptane (B) is greater than the n-heptane flow rate in the upper feed F_1. This means that some of the n-heptane in the distillate must come from the lower feed F_2. Likewise, since the component bottoms flow for n-octane (C) is greater than the n-octane flow rate in the lower feed, some of the n-octane in the bottoms must come from the upper feed F_1. Therefore, in this MFMP column, components with intermediate relative volatilities do not follow the same flow pattern when the MFMP column is decomposed into two single columns. The second reason is that, as the original MFMP column is decomposed into two simple columns, we lose the possibility that stream BC may control the minimum reflux. This results in a relaxed version of the optimization problem presented in Online Appendix C, thereby leading to an optimal solution that is lower than the minimum reflux ratio obtained by solving the full problem. Therefore, we must consider the entire MFMP column as a whole when modeling its separation performance and determining its minimum reflux condition, using methods such as the one presented in this work.

6 | CONCLUSION

In this paper, we introduce the mathematical formulation that incorporates the model developed in the first article of the series[22] to determine the minimum reflux condition of MFMP columns for multicomponent distillation. When the full product specifications are given, an algorithmic procedure is developed to automatically determine the minimum reflux ratio or minimum reboiler vapor duty requirement. When some of the product specifications are not given to users a priori, an optimization model can be developed as an MINLP to simultaneously identify the minimum reflux ratio and the corresponding optimal product distributions. We present the use of both approaches to analyze the minimum reflux behavior of MFMP columns. In all case studies, our minimum reflux ratio results match very well with rigorous Aspen Plus simulation results.

In addition to validating the accuracy and usefulness of our proposed algorithmic and optimization frameworks, the second aim of these case studies is to reexamine some of the well-accepted design heuristics and modeling assumptions the distillation community has been relying on regarding how MFMP columns should be designed and operated. It turns out that some of these heuristics and assumptions need to be rewritten. In Example 1, we show a counterexample where placing a colder feed stream above a warmer feed stream, which follows the temperature profile within the column, actually leads to a higher minimum vapor duty requirement than if the feed stream locations are reversed. Thus, we must analyze all possible permutations of relative feed locations to determine the optimal feed stream arrangement. Our shortcut-based approach is particularly suitable for analyses like this compared to rigorous process simulations, which can be quite time-consuming to perform, especially as the number of feed streams and/or side-draw streams increases.

Another key finding is that decomposing an MFMP column into multiple simple columns and taking the largest individual minimum reflux ratios of each decomposed column using the classic Underwood method is not the correct approach to determine the minimum reflux ratio of the original MFMP column. In fact, such a column decomposition approach can lead to minimum reflux ratio values that significantly deviate from the true minimum reflux ratio. On the other hand, our shortcut-based approach considers the entire MFMP column as a whole, which is needed for accurately estimating the true minimum reflux ratio.

Finally, when a distillation column has one or more sidedraw streams, one of the sidedraw streams can control the separation at minimum reflux, even when they are all withdrawn as saturated liquid streams. This possibility has often been overlooked by the distillation community in the past due to the lack of fundamental understanding and systematic tools to model how sidedraws affect the minimum reflux operation of a multicomponent distillation column. The mathematical model and algorithms developed in this series have filled this gap, thus allowing practitioners to conduct rigorous, accurate analysis of columns with sidedraws for the first time. Overall, we believe that these new findings and insights will be helpful in synthesizing and operating energy-efficient, cost-competitive, and intensified MFMP columns for multicomponent distillation.

DATA AVAILABILITY STATEMENT

The liquid composition data obtained from rigorous Aspen Plus simulations are transformed into the equilateral triangular coordinate as shown in Figures 5, 8, and 10 to be visualized. The transformed liquid composition data are provided in the Supplementary Material. The procedure and specifications used to produce the pinch simplices for all column sections are provided in Algorithms 1 through 3 within the article. The optimal product distribution results in Table 1 are obtained by the MINLP formulation provided in Online Appendix C.

ORCID

Zheyu Jiang https://orcid.org/0000-0003-4747-0539
Rakesh Agrawal https://orcid.org/0000-0002-6746-9829

REFERENCES

1. Górak A, Olujić Z. *Distillation: Fundamentals and Principles*. Elsevier Inc.; 2014.
2. White DC. Optimize energy use in distillation. *Chem Eng Prog*. 2012; 2012(3):35-41.
3. US DOE Industrial Efficiency & Decarbonization Office. Manufacturing Energy and Carbon Footprints (2018 MECS). 2021.
4. US DOE. Industrial Decarbonization Roadmap. 2022.
5. Shah VH, Agrawal R. A matrix method for multicomponent distillation sequences. *AIChE J*. 2010;56(7):1759-1775.
6. Nallasivam U, Shah VH, Shenvi AA, Tawarmalani M, Agrawal R. Global optimization of multicomponent distillation configurations: 1. Need for a reliable global optimization algorithm. *AIChE J*. 2013;59(3):971-981.
7. Nallasivam U, Shah VH, Shenvi AA, Huff J, Tawarmalani M, Agrawal R. Global optimization of multicomponent distillation configurations: 2. Enumeration based global minimization algorithm. *AIChE J*. 2016;62(6):2071-2086.
8. Jiang Z, Agrawal R. Process intensification in multicomponent distillation: a review of recent advancements. *Chem Eng Res Design*. 2019; 147:122-145.
9. Zheyuand JG, Ramapriya M, Tawarmalani M, Agrawal R. Process intensification in multicomponent distillation. *Chem Eng Trans*. 2018; 69:841-846.
10. Agrawal R, Tumbalam GR. Misconceptions about efficiency and maturity of distillation. *AIChE J*. 2020;66(8):e16294.
11. Agrawal R, Yee TF. Heat pumps for thermally linked distillation columns: an exercise for argon production from air. *Ind Eng Chem Res*. 1994;33(11):2717-2730.
12. Nogaja A, Tawarmalani M, Agrawal R. Distillation electrification through optimal use of heat pumps. In: Manenti F, Reklaitis GV, eds. vol. 53 of Computer Aided Chemical Engineering*34th European Symposium on Computer Aided Process Engineering/15th International Symposium on Process Systems Engineering*. Elsevier; 2024:1297-1302.
13. Wankat PC. Multieffect distillation processes. *Ind Eng Chem Res*. 1993;32(5):894-905.
14. Agrawal R, Herron DM. Intermediate reboiler and condenser arrangement for binary distillation columns. *AIChE J*. 1998;44(6):1316-1324.
15. Agrawal R, Fidkowski ZT, Xu J. Prefractionation to reduce energy consumption in distillation without changing utility temperatures. *AIChE J*. 1996;42(8):2118-2127.
16. Agrawal R, Herron DM. Optimal thermodynamic feed conditions for distillation of ideal binary mixtures. *AIChE J*. 1997;43(11):2984-2996.
17. Jiang Z, Madenoor Ramapriya G, Tawarmalani M, Agrawal R. Minimum energy of multicomponent distillation systems using minimum additional heat and mass integration sections. *AIChE J*. 2018;64(9): 3410-3418.
18. Tumbalam Gooty R, Chavez Velasco JA, Agrawal R. Methods to assess numerous distillation schemes for binary mixtures. *Chem Eng Res Design*. 2021;172:1-20.
19. Chavez Velasco JA, Tawarmalani M, Agrawal R. Systematic analysis reveals thermal separations are not necessarily Most energy intensive. *Joule*. 2021;5(2):330-343.
20. Gilliland ER. Multicomponent rectification. *Ind Eng Chem*. 1940;32(8): 1101-1106.
21. Doherty MF. Conceptual design of distillation systems. *McGraw-Hill chemical engineering series*. McGraw-Hill; 2001.
22. Jiang Z, Tawarmalani M, Agrawal R. Minimum reflux calculation for multicomponent distillation in multi-feed, multi-product columns: mathematical model. *AIChE J*. 2022;68(12):e17929.
23. Mathew TJ, Tawarmalani M, Agrawal R. Relaxing the constant molar overflow assumption in distillation optimization. *AIChE J*. 2023;*69*(9):e18125.
24. Mathew TJ, Gooty RT, Tawarmalani M, Agrawal R. Quickly assess distillation columns. *Chem Eng Prog*. 2020;2020(12):27-34.
25. Mathew TJ, Tumbalam Gooty R, Tawarmalani M, Agrawal R. A simple criterion for feasibility of heat integration between distillation streams based on relative volatilities. *Ind Eng Chem Res*. 2021;60(28):10286-10302.
26. Tumbalam Gooty R, Mathew TJ, Tawarmalani M, Agrawal R. An MINLP formulation to identify thermodynamically-efficient distillation configurations. *Comput Chem Eng*. 2023;178:108369.
27. Jiang Z. A shortcut minimum reflux calculation method for distillation columns separating multicomponent homogeneous azeotropic mixtures. *Le Scientifique*. 2020;2020(1):17-25.
28. Taifan GSP, Maravelias CT. Optimization-based Azeotropic distillation system synthesis using geometric insights. *Ind Eng Chem Res*. 2023; 62(31):12220-12234.
29. Jiang Z, Mathew TJ, Zhang H, et al. Global optimization of multicomponent distillation configurations: global minimization of total cost for multicomponent mixture separations. *Comput Chem Eng*. 2019;126: 249-262.
30. Jiang Z, Chen Z, Huff J, Shenvi AA, Tawarmalani M, Agrawal R. Global minimization of total exergy loss of multicomponent distillation configurations. *AIChE J*. 2019;65(11):e16737.
31. Tawarmalani M, Sahinidis NV. A polyhedral branch-and-cut approach to global optimization. *Math Program*. 2005;103:225-249.
32. Madenoor RG, Mohit T, Rakesh A. Modified basic distillation configurations with intermediate sections for energy savings. *AIChE J*. 2014; 60(3):1091-1097.
33. Shah VH. *Energy Savings in Distillation Via Identification of Useful Configurations* (Ph.D. thesis). Purdue University; 2010.
34. Lucia A, Amale A, Taylor R. Distillation pinch points and more. *Comput Chem Eng*. 2008;32(6):1342-1364.
35. Lucia A, Taylor R. The geometry of separation boundaries: I. Basic theory and numerical support. *AIChE J*. 2005;52(2):582-594.
36. Underwood AJV. Fractional distillation of multicomponent mixtures. *Ind Eng Chem*. 1949;41(12):2844-2847.
37. Underwood AJV. Fractional distillation of multicomponent mixtures. *Chem Eng Prog*. 1948;44:603-614.
38. Levy SG, Doherty MF. Design and synthesis of homogeneous azeotropic distillations. 4. Minimum reflux calculations for multiple-feed columns. *Ind Eng Chem Fund*. 1986;25(2):269-279.
39. Sugie H, Lu B. On the determination of minimum reflux ratio for a multicomponent distillation column with any number of side-cut streams. *Chem Eng Sci*. 1970;25(12):1837-1846.
40. Glinos KN, Malone MF. Design of sidestream distillation columns. *Ind Eng Chem Proc Design Devel*. 1985;24(3):822-828.

SUPPORTING INFORMATION

Additional supporting information can be found online in the Supporting Information section at the end of this article.

How to cite this article: Jiang Z, Tawarmalani M, Agrawal R. Minimum reflux calculation for multicomponent distillation in multi-feed, multi-product columns: Algorithms and examples. *AIChE J*. 2025;e70016. doi:10.1002/aic.70016